Pergamon

Int. J. Heat Mass Transfer. Vol. 38, No. 9, pp. 1661–1674, 1995

0017-9310/95 $9.50+0.00

0017-9310(94)00289-4

Vortex flow and thermal characteristics in mixed convection of air in a horizontal rectangular duct: effects of the Reynolds and Grashof numbers

C. C. HUANG and T. F. LIN†

Department of Mechanical Engineering, National Chiao Tung University, Hsinchu, Taiwan, Republic of China

(*Received* 1 *February* 1994 *and in final form* 10 *August* 1994)

Abstract—A three-dimensional unsteady numerical simulation was carried out to study the effects of Reynolds and Grashof numbers on the vortex flow structure and thermal characteristics in a buoyancy-induced time periodic mixed convective air flow through a bottom heated horizontal rectangular duct. The unsteady Navier–Stokes equations along with the continuity and energy equations were integrated by the Projection method with the convective and diffusive terms discretized by higher order finite difference schemes. Results for the Reynolds number varied from 1000 to 200 at a fixed Grashof number clearly show the splitting and merging of the longitudinal rolls. The flow destabilizes during the processes of roll merging and splitting. After the merging and splitting the flow gradually stabilizes as it moves downstream. For the Reynolds number at 100, stable thermal stratification appears in the upper half of the duct and the flow oscillation is significantly suppressed there.

1. INTRODUCTION

Forced convective heat transfer in ducts can be significantly modified by the buoyancy force when it is large compared with the inertia force. The degree of modification is determined by the values of the dominated parameters, namely, the Grashof, Reynolds and Prandtl numbers and duct geometry. Detailed understanding of this modification is important in many technological processes, such as cooling of microelectronic equipment, growth of single crystal from fluid phase, collection of solar energy, and many others. To unravel the complex mixed convective flow at a high buoyancy-to-inertia ratio, we numerically simulated the flow by performing unsteady and three-dimensional computation [1]. The results clearly show the buoyancy-induced transition from steady laminar to time periodic laminar, then to quasiperiodic transitional, and finally to weakly chaotic turbulent flow at increasing Grashof number for air flow through a bottom-heated horizontal rectangular duct with the Reynolds number fixed at 500. In a continuing effort, the present study intends to investigate the effects of the Reynolds and Grashof numbers on the flow and thermal characteristics. In what follows the literature on the mixed convective flow in a horizontal rectangular duct is briefly reviewed. A detailed review is available in a previous study [1].

Because of the limited availability of the computation facility to calculate the complex three-dimensional unsteady vortex flow considered here, most early studies [2–4] relied on experimental measurements to deduce the flow and thermal characteristics. Other studies [5, 6] used linear stability theory to predict the critical Rayleigh number for the onset of vortex flow. Besides, a numerical solution was attempted by Incropera and his colleagues [7, 8] for steady vortex flow. The above studies primarily focused on the large aspect ratio duct ($A > 10$) in order to simulate the flow in a plane channel. In spite of these studies the detailed processes on the formation of the vortex flow and the merge and splitting of the longitudinal vortex rolls are still poorly understood, especially for a finite aspect ratio duct in which the presence of the side walls can greatly change the vortex flow structure.

Considered in the present study is a mixed convective air flow in a bottom heated horizontal rectangular duct which is thermally well insulated, as schematically shown in Fig. 1. Initially, at time $t < 0$ the flow in the entire duct is fully developed and isothermal at T_e. At time $t = 0$ a uniform heat flux q''_w is suddenly imposed on the bottom wall over a finite

† Author to whom correspondence should be addressed.

NOMENCLATURE

A aspect ratio, b/d
b, d width and height of the duct
g gravitational acceleration
Gr modified Grashof number, $g\beta q''_w d^4/kv^2$
h local convection heat transfer coefficient
k thermal conductivity
l, L dimensional and dimensionless length of the heated plate, l/d
Nu Nusselt number, hd/k
P, p_m dimensionless and dimensional dynamic pressures, $p_m/\rho\overline{w_e}^2$
Pr Prandtl number, v/α
q''_w wall heat flux
Re Reynolds number, $\overline{w_e}d/v$
t, τ dimensional and dimensionless time, $t/(d/\overline{w_e})$
T, θ dimensional and dimensionless temperatures, $(T-T_e)/(q''_w d/k)$
u, v, w velocity components in x, y, z directions.
U, V, W dimensionless velocity components in X, Y, Z directions, $u/\overline{w_e}$, $v/\overline{w_e}$ and $w/\overline{w_e}$
x, y, z Cartesian coordinates
X, Y, Z dimensionless Cartesian coordinates, x/d, y/d and z/d
Z^+ modified Z coordinate, $Z/(Re\ Pr)$.

Greek symbols
α thermal diffusivity
β thermal expansion coefficient
v kinematic viscosity
ρ density.

Subscripts
e values at the duct inlet
fd fully developed
p period
w of wall qualitics.

Superscripts
$-$ average value
$*$ provisional value
n value at the nth time step.

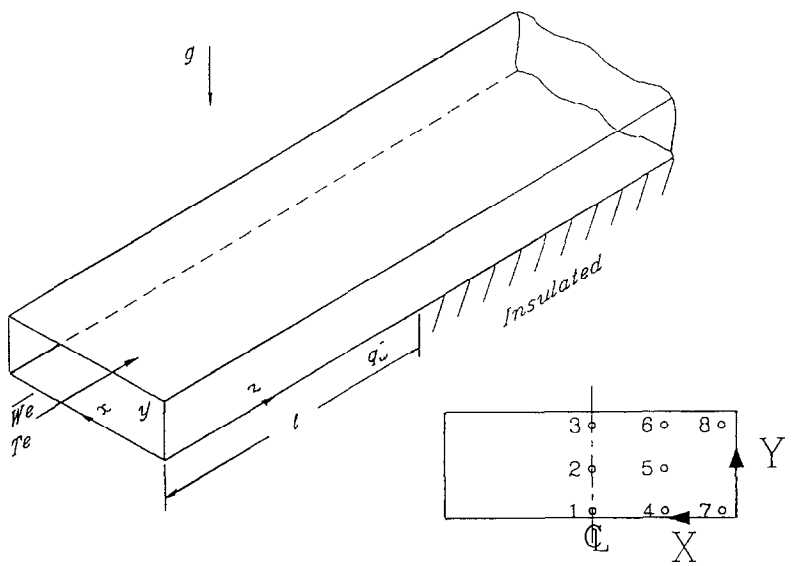

Fig. 1. Schematic of the physical system and the detection points at a cross-section. The X and Y coordinates at various points are as follows: 1—(2, 0.08); 2—(2, 0.5); 3—(2, 0.92); 4—(0.96, 0.08); 5—(0.96, 0.5); 6—(0.96, 0.92); 7—(0.32, 0.08); 8—(0.32, 0.92).

length l. This heat input produces upward buoyancy which is normal to the forced flow direction and hence can result in complex vortex flow structure. This study numerically investigates the effects of the Reynolds and Grashof numbers on the evolution of the vortex flow structure and associated heat transfer at high Grashof numbers, so that the flow does not reach steady state.

2. MATHEMATICAL FORMULATION AND SOLUTION METHOD

2.1. *Mathematical formulation*

Basic nondimensional equations describing the time evolution of a three-dimensional mixed convective flow of a Boussinesq fluid in a bottom-heated horizontal rectangular duct are

$$\frac{\partial U}{\partial X}+\frac{\partial V}{\partial Y}+\frac{\partial W}{\partial Z}=0 \tag{1}$$

$$\frac{\partial U}{\partial \tau}+U\frac{\partial U}{\partial X}+V\frac{\partial U}{\partial Y}+W\frac{\partial U}{\partial Z}=-\frac{\partial P}{\partial X}+\frac{1}{Re}\left[\frac{\partial^2 U}{\partial X^2}+\frac{\partial^2 U}{\partial Y^2}+\frac{\partial^2 U}{\partial Z^2}\right] \tag{2}$$

$$\frac{\partial V}{\partial \tau}+U\frac{\partial V}{\partial X}+V\frac{\partial V}{\partial Y}+W\frac{\partial V}{\partial Z}=-\frac{\partial P}{\partial Y}+\frac{1}{Re}\left[\frac{\partial^2 V}{\partial X^2}+\frac{\partial^2 V}{\partial Y^2}+\frac{\partial^2 V}{\partial Z^2}\right]+\frac{Gr}{Re^2}\theta \tag{3}$$

$$\frac{\partial W}{\partial \tau}+U\frac{\partial W}{\partial X}+V\frac{\partial W}{\partial Y}+W\frac{\partial W}{\partial Z}=-\frac{\partial P}{\partial Z}+\frac{1}{Re}\left[\frac{\partial^2 W}{\partial X^2}+\frac{\partial^2 W}{\partial Y^2}+\frac{\partial^2 W}{\partial Z^2}\right] \tag{4}$$

$$\frac{\partial \theta}{\partial \tau}+U\frac{\partial \theta}{\partial X}+V\frac{\partial \theta}{\partial Y}+W\frac{\partial \theta}{\partial Z}=\frac{1}{Re\,Pr}\times\left[\frac{\partial^2 \theta}{\partial X^2}+\frac{\partial^2 \theta}{\partial Y^2}+\frac{\partial^2 \theta}{\partial Z^2}\right] \tag{5}$$

subject to the following initial and boundary conditions:

$$\text{at}\quad \tau=0 \quad \text{or} \quad Z=0 \quad U=V=\theta=0$$

$$W=W_{fd}=\left(\frac{m_1+1}{m_1}\right)\left(\frac{m_2+1}{m_2}\right)[1-(|2Y-1|)^{m_2}]\times\left[1-\left(\left|\frac{2X}{A}-1\right|\right)^{m_1}\right] \tag{6}$$

where the values of m_1 and m_2 depend on the aspect ratio [9], for $\tau>0$,

$$\text{at}\quad Z=2L \quad \frac{\partial U}{\partial Z}=\frac{\partial V}{\partial Z}=\frac{\partial \theta}{\partial Z}=\frac{\partial W}{\partial Z}=0 \tag{7}$$

$$\text{at}\quad Y=0 \quad \text{and} \quad 0\leqslant Z\leqslant L \quad \frac{\partial \theta}{\partial Y}+1=U=V=W=0 \tag{8}$$

$$\text{at all other surfaces}\quad \frac{\partial \theta}{\partial n}=U=V=W=0 \tag{9}$$

where n is a unit normal to a surface. The above equations are in terms of the following nondimensional variables:

$$X=x/d \quad Y=y/d \quad Z=z/d$$

$$U=u/\overline{w_e} \quad V=v/\overline{w_e} \quad W=w/\overline{w_e}$$

$$Re=\overline{w_e}d/\nu \quad Pr=\nu/\alpha \quad Gr=\frac{(g\beta q''_w d^4)}{(k\nu^2)}$$

$$\theta=\frac{(T-T_e)}{(q''_w d/k)} \quad A=b/d \quad \tau=\frac{t}{(d/\overline{w_e})}$$

$$P=\frac{p_m}{\rho \overline{w_e}^2}. \tag{10}$$

Note that in the above formulation an insulated section of length l is added to the exit end of the heated section to facilitate the prescription of the out-flow boundary conditions in the present elliptic flow analysis. This added section must be long enough so that the specified downstream boundary condition, equation (7), is suitable. Care is always taken in the solution process to examine whether this added length is long enough or not.

The local Nusselt number on the heated plate measuring the convective heat transfer from the plate to the flow in the duct is defined as

$$Nu=\frac{hd}{k}=\frac{q''_w}{T_w-T_e}\frac{d}{k}=\frac{1}{\theta_w}. \tag{11}$$

The spanwise averaged Nusselt number is defined as

$$\overline{Nu(Z)}=\frac{\bar{h}d}{k}=\frac{1}{A}\int_0^A \frac{q''_w d}{(T_w-T_e)k}\,dX \tag{12}$$

where A is the aspect ratio.

2.2. *Solution method*

The time-dependent three-dimensional governing equations were solved numerically by the Projection method [10] on a staggered grid system. This fractional step method, which was also used in the previous study [1], consists of two steps. First, the pressure gradient is ignored and a provisional velocity field is predicted by the simple explicit method [11]. Second, the provisional velocity is corrected by including the pressure effect and enforcing the mass conservation. The resulting pressure Poisson equation was solved by a vectorized SOR method. The energy equation was also solved by the simple explicit method. To ensure the converged solution, the CFL condition that the Courant number must be less than unity was imposed in selecting the time step size. In the spatial discretization the convective and diffusive terms were respectively approximated by the third-order upwind and fourth-order central difference schemes. These higher order schemes can produce stable and accurate results. In the grid distribution 41–61 nodes were placed uniformly in each coordinate direction. Computations were started from the beginning of the transient to the final steady state or to the statistical state when the flow does not reach steady state at large τ.

Stringent program tests were carried out in the previous study [1] to verify the proposed solution

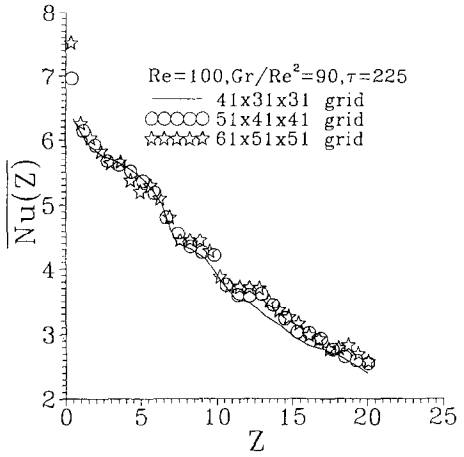

Fig. 2. Comparison of the spanwise averaged Nusselt number at the same time from various grids for $Pr = 0.7$, $Re = 100$, $Gr/Re^2 = 90$, $A = 4$ and $L = 20$.

method. Good agreement between the present predictions and published results in the literature was shown by comparing our predictions with the analytic and/or numerical results for the limiting case of pure forced convection and the experimental data for the steady mixed convective vortex flow in a horizontal flat duct [3, 4]. To further validate the solution method, grid independence tests were conducted here. Figure 2 shows the sample results for the spanwise averaged Nusselt number for a typical case with a time-periodic flow induced in the duct for $Re = 100$ and $Gr/Re^2 = 90$ from such tests. Good agreement is found for the predictions from various grid densities. More details on the solution method are available from the previous study [1].

It is important to ensure the predicted flow oscillation does not result from numerical instability. When an oscillatory flow appears in the computation for a given set of parameters, the Reynolds number was raised by a certain amount and the computation is continued. The results indicate that the vortex flow gradually becomes steady for a large rise in Re. Thus the predicted oscillatory flow is due to physical instability instead of numerical artifacts.

3. RESULTS AND DISCUSSION

In the present numerical simulation the Reynolds number was first systematically varied over wide ranges so that the flow of air ($Pr = 0.72$) changes from a steady laminar state to a turbulent chaotic state at fixed Grashof numbers, duct aspect ratio ($A = 4$) and heated section length ($L = 20$). Besides, the Grashof number was also varied over wide ranges at $Re = 100$, again for $A = 4$ and $L = 20$. Only a small sample of results will be presented here to mainly delineate the effects of the Reynolds and Grashof numbers on the vortex flow structure and associated heat transfer characteristics.

Results for Gr fixed at 2.5×10^6 and Re reduced from 1000 are presented first. The results indicate that, for $700 \leqslant Re \leqslant 1000$, steady vortex flow in the form of longitudinal rolls prevails after the initial transient in the downstream portion of the heated section. When Re is reduced to 600, temporal flow oscillation is seen near the duct exit at large τ. Reducing the Reynolds number further causes the oscillatory flow to be prevalent over a larger downstream region in the heated section.

Continuing reduction of Re to 500 and 400 results in some unusual flow characteristics which deserve special attention. To illustrate these special flow characteristics, Fig. 3(a)–(d) shows the time histories of the temperature θ and axial velocity W at large τ at eight detection points, specified in Fig. 1 at four selected cross-sections. Note that the flow oscillates periodically with single fundamental frequency f ($= 1/\tau_p = 0.14$) in the entire duct, where τ_p is the nondimensional period of the oscillations. But the amplitude of the oscillation shows nonmonotonic variation with the axial distance. This defies the general conception that the flow gradually becomes disordered when travelling downstream. Specifically, at locations 1, 2 and 3 near the central vertical plane at $X = A/2$, the flow is steady in the duct. Near the side walls (locations 7 and 8), large oscillation is induced in the entry region [Fig. 3(a) and (b)] and decays significantly for $Z > 7.1$. In regions away from the central plane and side walls the oscillation increases with the axial distance for $Z < 7.1$. Downstream of it the oscillation decays. The consequence of this unusual decay in the flow oscillation can be attributed to the unusual axial flow development displayed in Fig. 4, in which, due to the flow being symmetric with respect to the central vertical plane, the isotherms in the left half and the streamlines of the secondary flow in the right half of the duct are plotted together at selected cross-sections at selected time instants in a typical period. These results clearly show that four pairs of vortex rolls in the entry region gradually merge into two pairs at $Z \approx 6.0$. Comparing the results in Fig. 4 with those in Fig. 3 suggests that, during the process of the cell merging, the flow is destablized with amplifying oscillation, especially at the cell interfaces (locations 4–6). After the cell merges the flow gradually stablizes, as is evident from the periodic flow patterns in Fig. 4. It is of interest to mention that the change of the flow pattern with time is rather small after the cell merges ($Z \geqslant 6.0$).

At an even lower Reynolds number, more structural changes in the vortex flow appear. The periodic flow patterns for $Re = 200$ are demonstrated in Fig. 5. Note that two pairs of longitudinal rolls occupy nearly the entire heated section of the duct, except in the exit region where the roll splitting takes place and two new pairs of rolls become visible. This roll splitting then destablizes the flow. The time records of W and θ given in Fig. 6 show that the flow in the entry region oscillates periodically at a frequency of 0.267 in a small amplitude [Fig. 6(a)]. Slightly downstream the

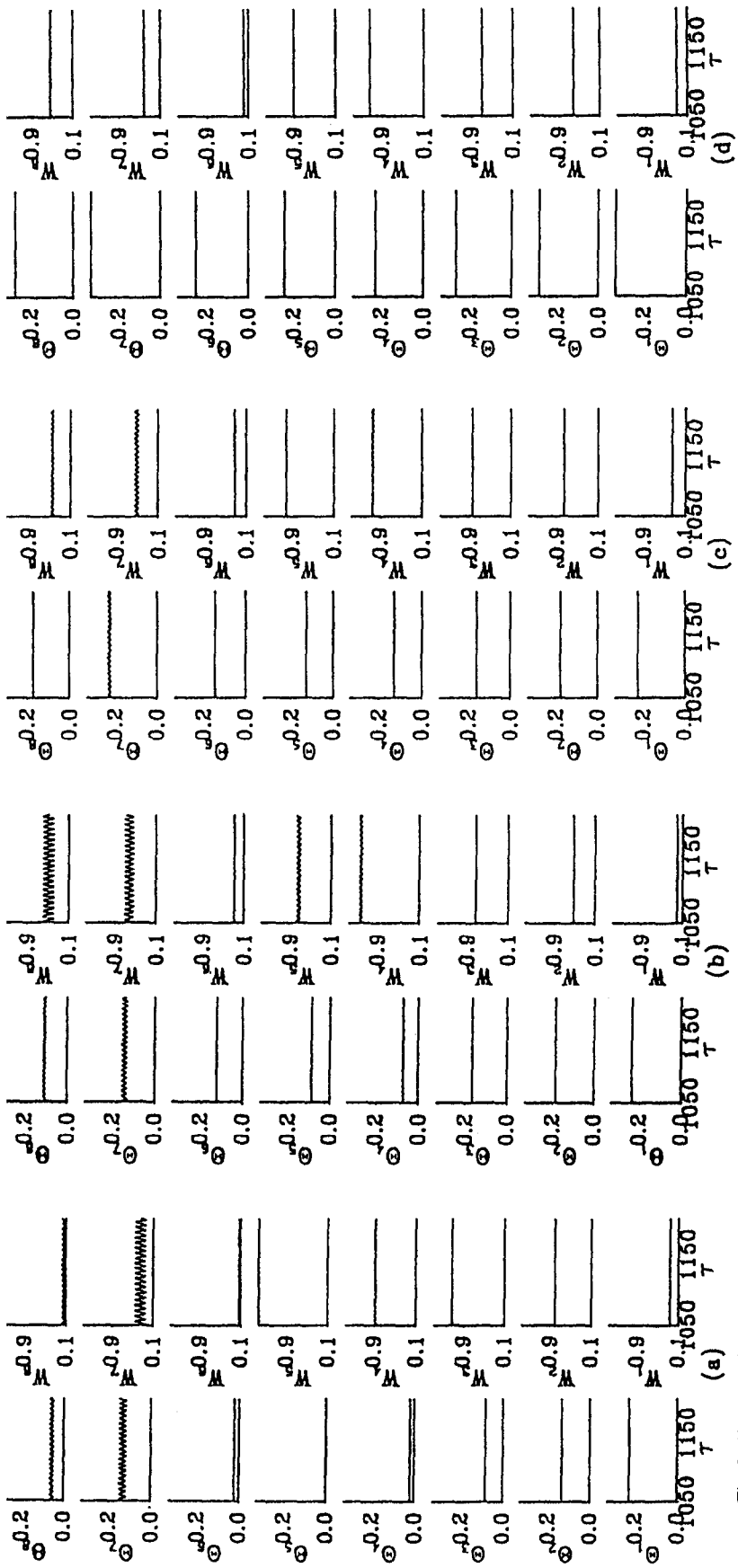

Fig. 3. Time samples for W and θ at eight detection points for $Re = 400$, $Gr/Re^2 = 15.625$ at : (a) $Z = 3.23$; (b) $Z = 7.10$; (c) $Z = 10.97$; (d) $Z = 18.70$. θ_i and W_i respectively denote θ and W at detection points i and j.

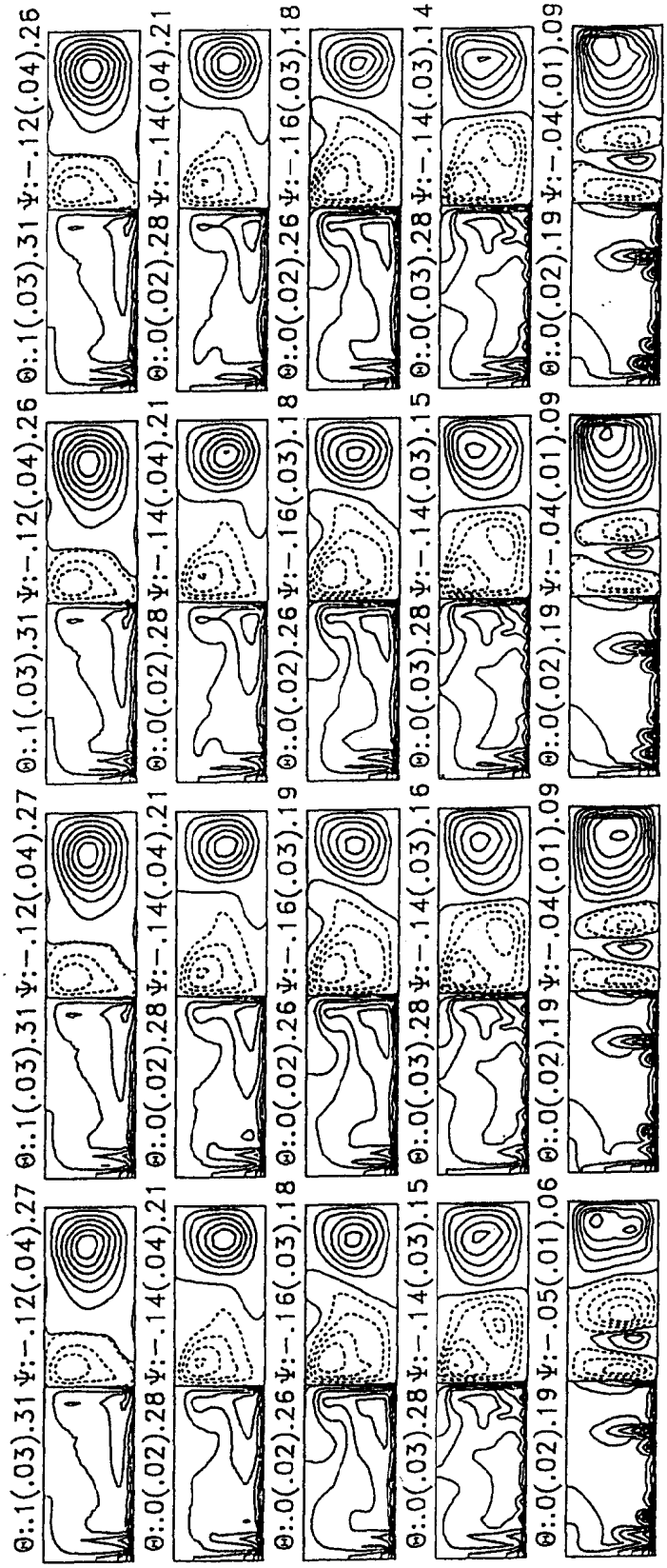

Fig. 4. Periodic flow patterns at a large τ for $Gr/Re^2 = 15.625$ and $Re = 400$ at: (a) $Z = 1.29$; (b) $Z = 3.87$; (c) $Z = 6.45$; (d) $Z = 9.03$; and (e) $Z = 14.19$. The period of the oscillation is about 7.153.

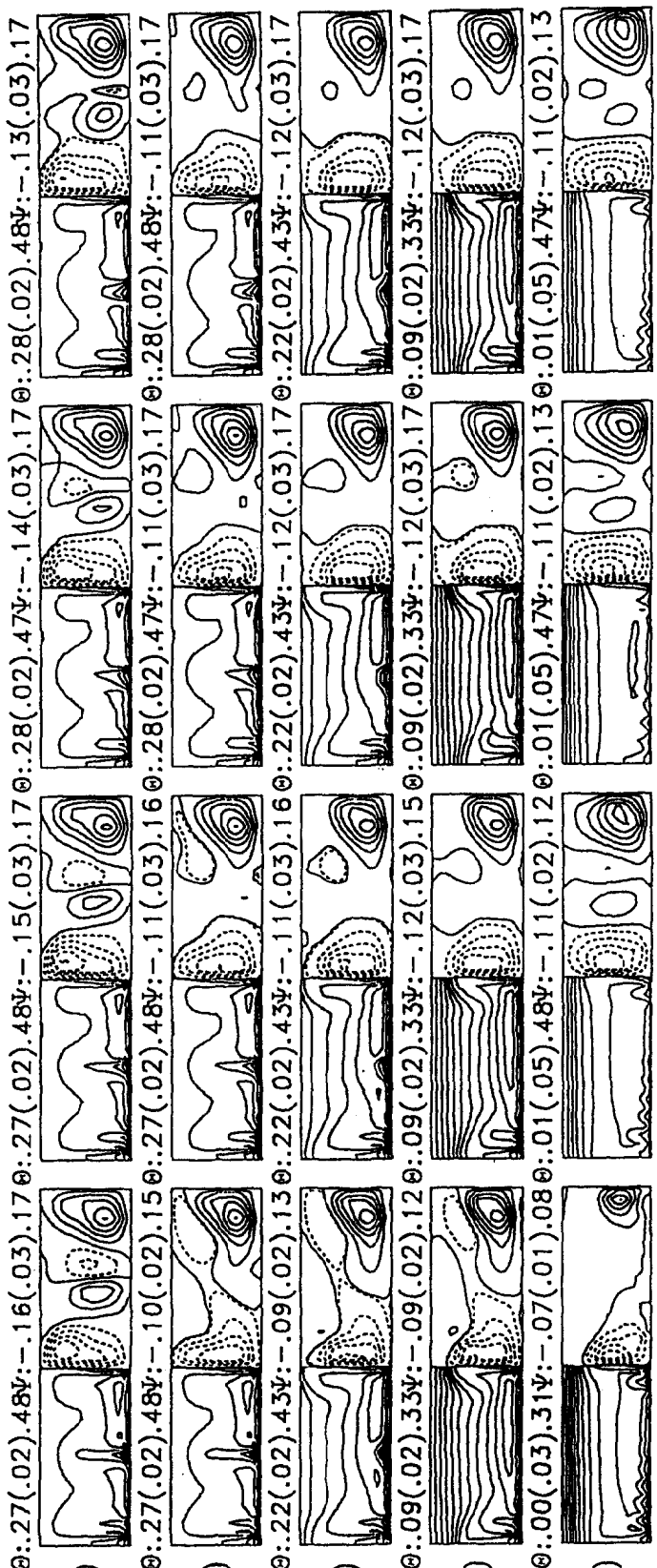

Fig. 5. Periodic flow patterns at a large τ for $Gr/Re^2 = 62.5$ and $Re = 200$ at: (a) $Z \approx 1.29$; (b) $Z \approx 6.45$; (c) $Z = 11.61$; (d) $Z \approx 14.19$; and (e) $Z \approx 16.77$. The period of the oscillation is about 3.7453.

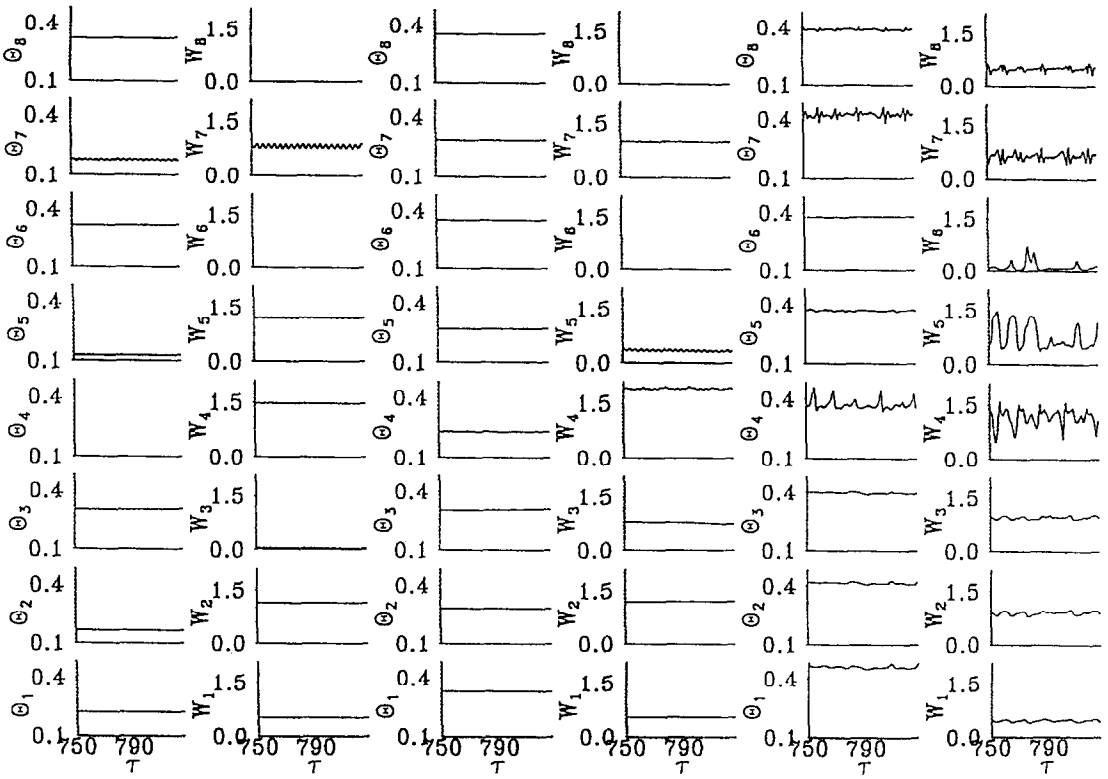

Fig. 6. Time samples for W and θ at eight detection points for $Re = 200$, $Gr/Re^2 = 62.5$ at: (a) $Z = 3.23$; (b) $Z = 10.97$; (c) $Z = 18.70$.

oscillation amplitude decays somewhat, but some nonperiodic components are observed [Fig. 6(b)]. Near the duct exit the oscillation intensifies drastically and becomes chaotic [Fig. 6(c)] because of the roll splitting. As Re is further lowered to 100, the flow becomes highly unstable and fluctuates violently, except near the duct inlet. Hence we failed to obtain a converged solution.

It is of interest to point out that the buoyancy-induced unsteady mixed convective vortex flow at low Reynolds numbers possesses some other unique characteristics. To explore these characteristics, a series of computations was conducted for Re fixed at 100 and Gr gradually raised. The results from these computations indicate that the flow finally attains steady state for $Gr/Re^2 \leqslant 40$ or $Gr \leqslant 4.0 \times 10^5$. Figure 7 shows that, at a very low buoyancy ($Gr/Re^2 \leqslant 15$ or $Gr \leqslant 1.5 \times 10^5$), there is a single pair of buoyancy-driven longitudinal rolls occupying the entire duct at steady state. Thus, the roll size is about twice in the spanwise dimension as that in the vertical direction. When the buoyancy is slightly raised to the range of Gr/Re^2 between 20 and 40, two pairs of longitudinal rolls are induced at steady state. The wavelength of the rolls is about $2d$. As Gr/Re^2 is raised to 50, flow starts to oscillate periodically in the region near the duct exit ($Z \geqslant 14.84$), but there are still only two pairs of vortices in the duct, like those observed at lower buoyancy. For a higher Gr/Re^2 the flow oscillation appears in the region close to the duct inlet, and the region in which steady flow prevails is smaller and hence confined to the duct entry. For instance the results for $Gr/Re^2 = 90$ are shown in Figs. 8 and 9. The periodic vortex flow patterns in Fig. 8 suggest that, in the region for Z between 1.5 and 10.0, the rolls split over a certain interval of time in a period, but they merge later in another interval of time. Furthermore, at a given time instant the cells may split near the duct inlet and merge downstream. This complicated temporal and spatial variation in the vortex flow structure causes the flow to be highly fluctuating, as is evident from the time histories of W and θ in Fig. 9. A power spectrum density analysis of the data in Fig. 9 indicates that the flow in the entire duct oscillates at a single fundamental frequency $f_1 = 0.093$ and the oscillations at various locations can be characterized by this frequency and its harmonics. Comparing the oscillation amplitudes in Fig. 9(a)–(c) shows that the oscillation amplifies in the first half of the duct ($3.23 \leqslant Z \leqslant 10.97$), but decays in the secondary half ($Z > 11.0$). It is worth mentioning from the results in Fig. 9(a) and (b) that the flow is nearly

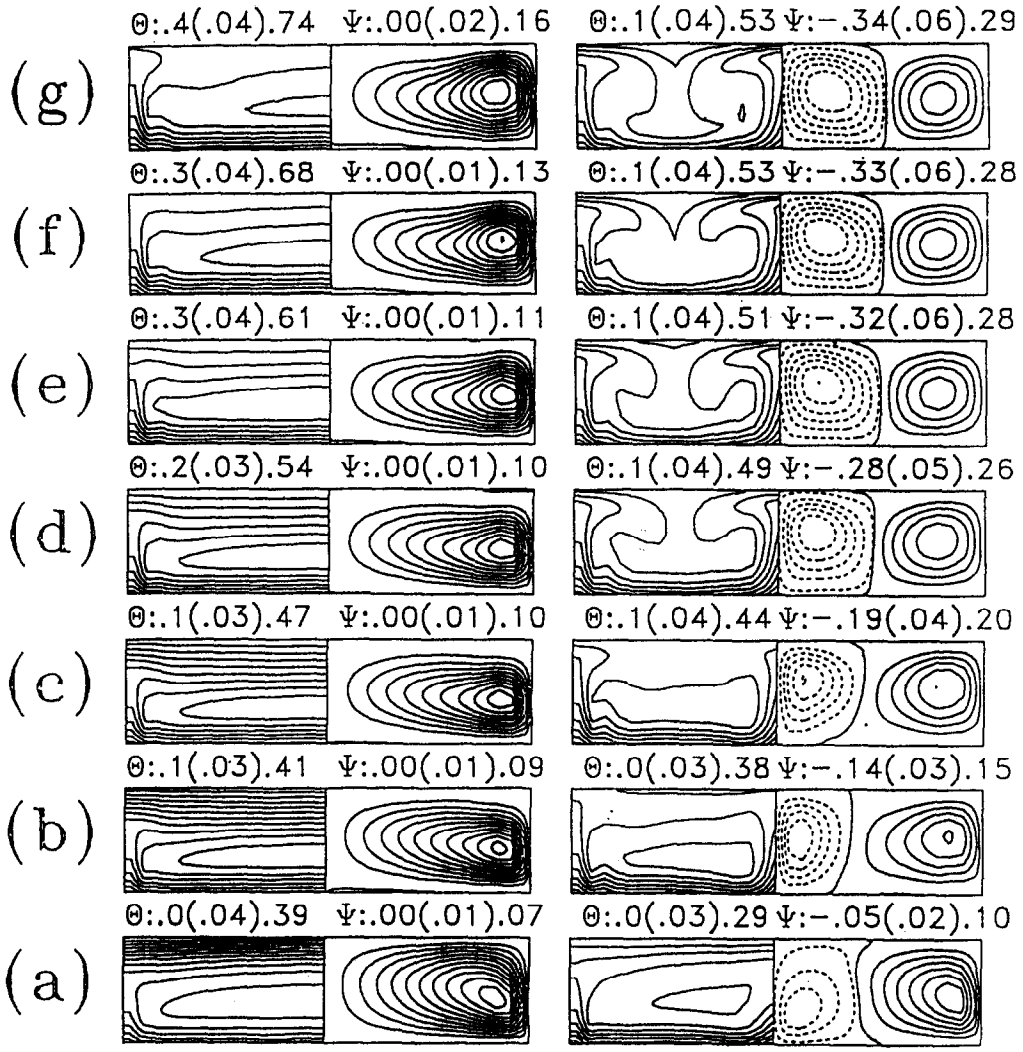

Fig. 7. Steady flow patterns at selected cross-sections for $Re = 100$, $Gr/Re^2 = 15$ and 20 at: (a) $Z = 1.29$; (b) $Z = 3.87$; (c) $Z = 6.45$; (d) $Z = 9.03$; (e) $Z = 11.61$; (f) $Z = 14.19$; (g) $Z = 16.77$.

steady at locations 3, 6 and 8 in the region adjacent to the duct top. This is conjectured to result from the stable thermal stratification in this region, as is evident from the isotherms in Fig. 8. This stable stratification also confines the cell motion in the lower half of the duct. To further elucidate the complicated flow motion, the phase space trajectories which relate the motion of three velocity components U, V and W at large τ are plotted in Fig. 10 for the eight detection points at $Z = 10.97$. At each location a limiting cycle (repeated curves) results, reflecting the flow at this location being completely periodic. These curves clearly show that the relative motion of U, V and W driven by the vertical buoyancy is rather complex, especially at locations 5–8.

Results for the distributions of the bottom plate temperature and local Nusselt number, which are of value to thermal design, are given in Fig. 11 at selected time instants for the three selected cases discussed above. The results obviously reflect the buoyancy-induced vortex roll structures. Note that the time variation of Nu with time is much smaller than that of velocity and temperature, due to the fact that Nu is an integral property of the flow.

Finally, the condition for the onset of the Hopf bifurcation, a transition from a steady to time-per-

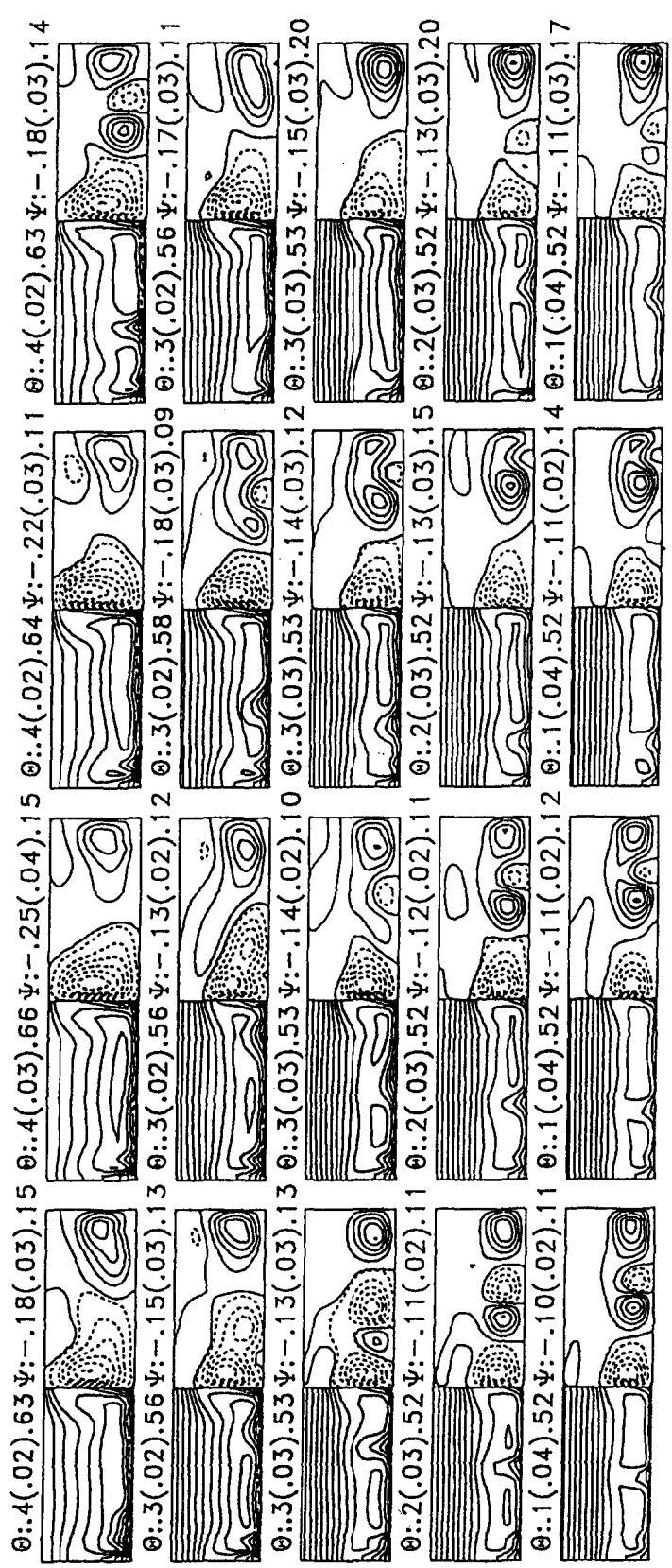

Fig. 8. Periodic flow patterns at a large τ for $Gr/Re^2 = 90$ and $Re = 100$ at: (a) $Z = 1.29$; (b) $Z = 3.87$; (c) $Z = 6.45$; (d) $Z = 9.03$; and (e) $Z = 14.19$. The period of the oscillation is about 12.99.

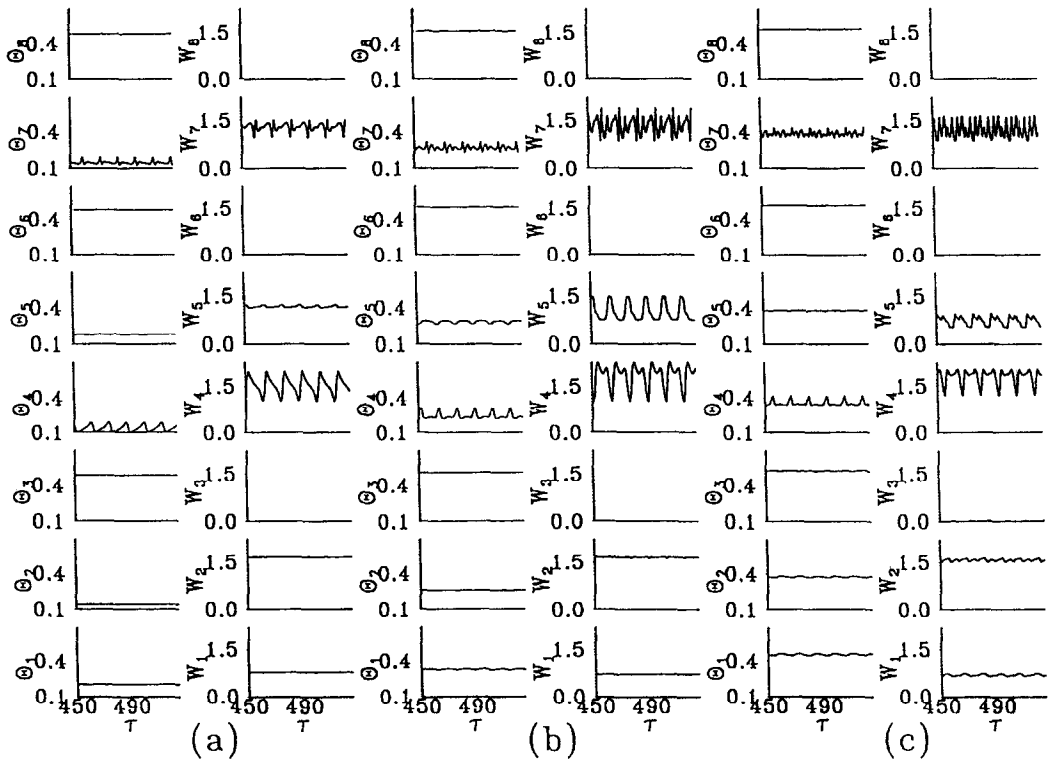

Fig. 9. Time samples for W and θ at eight detection points for $Re = 100$, $Gr/Re^2 = 90$ at: (a) $Z = 3.23$; (b) $Z = 10.97$; (c) $Z = 18.70$.

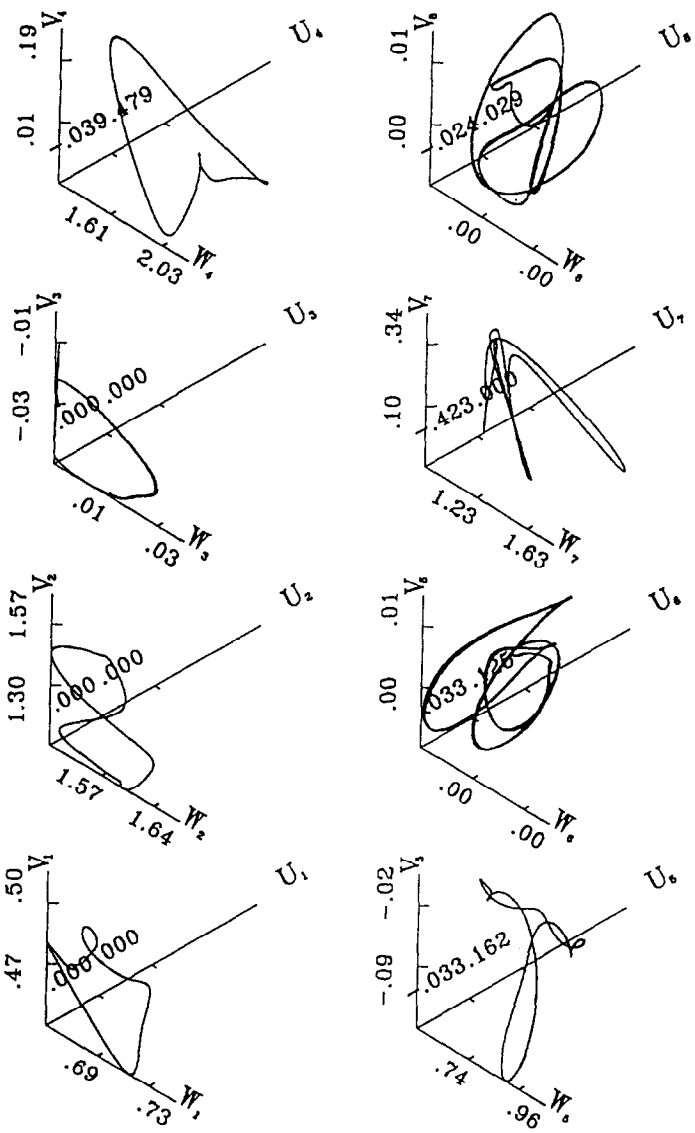

Fig. 10. Phase space trajectories of U, V and W at eight detection points for $Re = 100$, $Gr/Re^2 = 90$ and $Z = 10.97$.

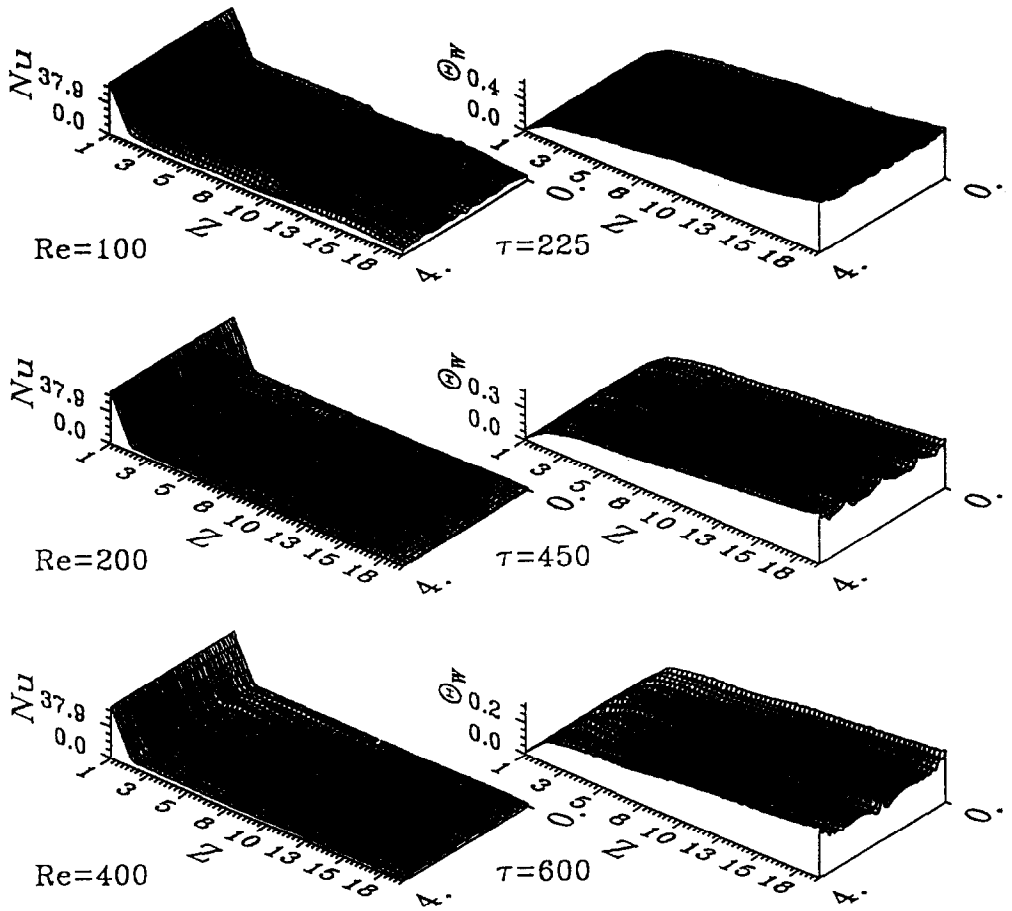

Fig. 11. The local Nusselt number distributions on the heated bottom plate for: (a) $Re = 100$, $Gr/Re^2 = 90$; (b) $Re = 200$, $Gr/Re^2 = 62.5$; and (c) $Re = 400$, $Gr/Re^2 = 15.625$ at large τ.

iodic state deduced from the large amount of the computer data, can be correlated as

$$Ra^*(Z^+)^{0.15} = 2.62 \times 10^5 \quad (13)$$

where $Z^+ = Z/(Re\ Pr)$.

4. CONCLUDING REMARKS

Through a direct three-dimensional unsteady numerical simulation, the splitting and merging of the longitudinal rolls were predicted in a high Grashof and/or low Reynolds number mixed convective flow of air in a bottom-heated horizontal rectangular duct. These complicated structural changes in the vortex flow have substantial effects on the fluctuating characteristics of the flow. Usually, the flow becomes more unsteady during the processes of roll splitting and merging. But after the splitting and merging the flow gradually stabilizes as it moves downstream. At low Reynolds numbers and high Grashof numbers stable thermal stratification results in the upper half, which in turn suppresses the roll size and stablizes the flow there.

Finally, it was recognized during the course of this investigation that the change in vortex flow structure is more severe in a large aspect ratio (wider) channel, since it provides larger lateral space for cells to move. Besides, the effects of duct inclination are expected to be significant. The evolution of vortex flow in mixed convection of water is also important in various applications. Preliminary computations on these problems support these statements.

Acknowledgement—The financial support of this study by the engineering division of Nation Science Council of Taiwan through the contract NSC83-0404-E009-054 is greatly appreciated. The support of the present computation by the National Center for High-performance Computing and by the computer center of the National Chiao Tung University, Taiwan is also acknowledged.

REFERENCES

1. C. C. Huang and T. F. Lin, Buoyancy-induced flow transition in mixed convective flow of air through a bottom-heated horizontal rectangular duct, *Int. J. Heat Mass Transfer* **37**, 1235–1255 (1994).
2. Y. Kamotani and S. Ostrach, Effect of thermal instability on thermally developing laminar channel flow, *J. Heat Transfer* **98**, 62–66 (1976).
3. K. C. Chiu, J. Ouazzani and F. Rosenberger, Mixed convection between horizontal plates—II. Fully

developed flow, *Int. J. Heat Mass Transfer* **30,** 1655–1662 (1987).
4. J. R. Maughan and F. P. Incropera, Regions of heat transfer enhancement for laminar mixed convection in a parallel plate channel, *Int. J. Heat Mass Transfer* **33,** 555–570 (1990).
5. G. J. Hwang and K. C. Cheng, Convective instability in the thermal entrance region of a horizontal parallel-plate channel heated from below, *J. Heat Transfer* **95,** 72–77 (1973).
6. F. S. Lee and G. J. Hwang, Transient analysis on the onset of thermal instability in the thermal entrance region of a horizontal parallel plate channel, *J. Heat Transfer* **113,** 363–370 (1991).
7. H. V. Mahaney, S. Ramadhyani and F. P. Incropera, Numerical simulation of three-dimensional mixed convection heat transfer from an array of discrete heat sources in a horizontal rectangular duct, *Numer. Heat Transfer A* **16,** 267–286 (1989).
8. J. R. Maughan and F. P. Incropera, Fully developed mixed convection in a horizontal channel heated uniformly from above and below, *Numer. Heat Transfer A* **17,** 417–430 (1990).
9. R. K. Shah and A. L. London, *Laminar Flow Force Convection in Ducts*, pp. 196–198. Academic Press, New York (1978).
10. A. J. Chorin, Numerical solution of the Navier–Stokes equations, *J. Math. Comput.* **22,** 742–762 (1968).
11. R. Peyret and T. D. Taylor, *Computational Methods for Fluid Flow*, Chap. 6. Springer, New York (1983).